

Magnetic and structural properties of BiFeO₃ thin films grown epitaxially on SrTiO₃/Si substrates

Ryan P. Laughlin; Daniel A. Currie; Rocio Contreras-Guererro; Aruna Dedigama; Weerasinghe Priyantha; Ravindranath Droopad; Nikoleta Theodoropoulou; Peng Gao; Xiaoqing Pan



Journal of Applied Physics 113, 17D919 (2013)

<https://doi.org/10.1063/1.4796150>



View Online



Export Citation

CrossMark

Articles You May Be Interested In

Self-assembled epitaxial BiFeO₃-Ni_{0.65}Zn_{0.35}Al_{0.8}Fe_{1.2}O₄ nanobelt heterostructures on SrTiO₃: Control of magnetic anisotropy, easy axis, and coercivity

Journal of Applied Physics (September 2019)

First-principles prediction of a two dimensional electron gas at the BiFeO₃/SrTiO₃ interface

Appl. Phys. Lett. (August 2011)

Multiferroics properties in BiFeO₃/CoFe₂O₄ heterostructures thin films deposited on (111) SrTiO₃

AIP Conference Proceedings (May 2016)

Webinar

Boost Your Signal-to-Noise Ratio with Lock-in Detection



Sep. 7th – Register now



Zurich Instruments

Magnetic and structural properties of BiFeO₃ thin films grown epitaxially on SrTiO₃/Si substrates

Ryan P. Laughlin,¹ Daniel A. Currie,¹ Rocio Contreras-Guererro,¹ Aruna Dedigama,¹ Weerasinghe Priyantha,¹ Ravindranath Droopad,¹ Nikoleta Theodoropoulou,^{1,a)} Peng Gao,² and Xiaoqing Pan²

¹Department of Physics, Texas State University-San Marcos, 601 University Drive, San Marcos, Texas 78666, USA

²Material Science and Engineering, University of Michigan, 2105 H. H. Dow Bldg, 2300 Hayward Street, Ann Arbor, Michigan 48109, USA

(Presented 18 January 2013; received 5 November 2012; accepted 19 December 2012; published online 11 April 2013)

The integration of oxides with semiconductors is important for the technological advancement of the next generation electronics. Concomitant ferroelectric and antiferromagnetic (AF) behavior is demonstrated in single crystal BiFeO₃ (BFO) films grown on 20 nm SrTiO₃ (STO) virtual substrates on Si(100) using molecular beam epitaxy (MBE). STO thin films are grown in an oxide MBE chamber by co-deposition of Sr, Ti, and molecular O₂. Careful control of the O₂ during nucleation produced commensurate growth of STO on Si. The sequence of the steps allows for the suppression of an amorphous SiO₂ layer. This STO(20 nm)/Si structure was used as a virtual substrate for MBE deposition of BFO on Si without breaking vacuum. BFO was deposited using Fe and O₂ plasma with an overpressure of Bi flux, the growth rate was controlled by the incoming Fe flux. The reflection high energy electron diffraction image shows a 2-D growth front with a 6-fold surface reconstruction under optimized O₂ pressure of 5×10^{-8} mbar. Cross-sectional transmission electron microscopy (TEM) confirms the high crystallinity of the films and shows sharp, atomically flat interfaces. The selected area diffraction pattern (SADP) reveals that BFO grows in a distorted rhombohedral crystal structure. X-ray diffraction does not show formation of second phases and is consistent with the TEM and SADP results. The BFO films show AF behavior with a Neel temperature that exceeds 350 K, as expected ($T_N = 673$ K) and with a residual ferromagnetic behavior that decreases with film thickness and is consistent with the G-type AF due to the canted spins. The saturation magnetization per unit volume for a 40 nm thick film was 180 emu/cm³ at an in-plane magnetic field of 8 kOe. The ferroelectric behavior of the films was verified using piezoresponse force microscopy. © 2013 American Institute of Physics. [<http://dx.doi.org/10.1063/1.4796150>]

The field of multiferroics (materials in which any two of their magnetic, electric, or structural order parameters are coupled) has experienced a recent resurgence due to the stronger coupling between electric and magnetic orders in materials that have a spiral, canted incommensurate antiferromagnetic (AF) order. BiFeO₃ (BFO) is the most notable example; both its ferroelectric transition temperature, $T_c \sim 1100$ K, and AF Neel temperature, $T_N \sim 673$ K are well above room temperature and exhibits long-range coupling of the electric and magnetic degrees of freedom at room temperature.^{1,2} It has a high remnant polarization ($\sim 60 \mu\text{C}/\text{cm}^2$)¹ and because it does not contain lead (Pb), it is used as the active layer in prototype ferroelectric memory (Fujitsu).² The coupling between magnetic and electric signals has several potential applications such as electrical writing in magnetic data storage or magnetic tuning of the dielectric constants in filters.

The integration of oxides with semiconductors and especially Si is important for the technological advancement of the next generation electronics as they allow for additional functionalities to be monolithically integrated onto complementary metal oxide semiconductor (CMOS) devices. The

physical properties of oxides such as conductivity, magnetic behavior, and ferroelectricity can be enhanced with oxide crystallinity and can be tailored to applications.

So far, the most successful growth of a crystalline oxide on semiconductors that has been achieved is the perovskite SrTiO₃ (STO) on both Si and GaAs using molecular beam epitaxy (MBE)³⁻⁵ in the same system that the BFO thin films presented in this report were grown. Recently, strained, thin films of STO (up to 2.4 nm) grown by MBE on Si were reported to show ferroelectric behavior up to 300 K.⁶ Multiferroicity was demonstrated in single crystal BFO grown on STO substrates by MBE, Pulsed laser deposition (PLD), chemical methods and rf-sputtering. Most of the research frontier is on BFO films grown by PLD and the main scope is modulation of the ferroelectric properties by stress engineering through the use of different substrates.^{1,7} Here, we use MBE for both the BFO thin films and the virtual substrate of STO directly on Si(100) without breaking vacuum for the first time.

The X-ray photoelectron spectroscopy (XPS) emission data were taken *in-situ* before exposure to air using a Scienta 400 detector. The crystal structure of the films was determined by X-ray diffraction (XRD) with Cu K α radiation

^{a)}E-mail: ntheo@txstate.edu

after exposing the films to air. Cross-sectional transmission electron microscopy (TEM) specimens of thin films were prepared by mechanical polishing followed by argon ion milling, and characterized by an aberration-corrected STEM (JEOL 2100F with probe corrected) and high resolution TEM (JEOL 3011), respectively. The magnetic measurements were taken in a Quantum Design Physical Properties Measurement System (PPMS) using the vibrating sample magnetometer (VSM) option. The topography was taken using a Veeco-D3100 atomic force microscope, equipped with a Nanoscope IV. The ferroelectric behavior was characterized using piezoresponse force microscopy (PFM) by modifying the AFM setup and using a commercially available Ti/Pt coated silicon tip (MikroMasch-NSC35).

STO thin films were fabricated by co-deposition of Sr, Ti, and molecular oxygen using elemental sources for Sr and Ti with the Ti being evaporated from a high temperature effusion cell. The fluxes were adjusted for stoichiometric STO and the growth rate was determined from reflection high energy electron diffraction (RHEED) intensity oscillations. The pressure of the chamber was used as a measure of the incident oxygen flux. After removing the oxide from the Si substrate using a flux of Sr, the substrate was cooled to 500 °C and additional Sr was added to form a (2 × 1) structure. Growth was initiated at 200 °C after the introduction of oxygen into the chamber to the required pressure of 1×10^{-8} mbar. STO on Si(100) was deposited using the sequence of the steps outlined in Ref. 3 allowing for the suppression of an amorphous SiO₂ layer and 2-dimensional growth. A careful control of the oxygen during nucleation has been demonstrated to produce commensurate growth of SrTiO₃ on Si. This STO/Si structure also serves as a virtual substrate on which to deposit other functional oxides that cannot be grown directly on Si.

BFO like all other oxides cannot be grown directly on Si due to the high reactivity of Si with oxygen and the immediate formation of SiO₂. The thickness of STO was 20 nm for all samples presented here and the STO/Si structure was used as a virtual substrate for MBE deposition of BFO without breaking vacuum. To ensure complete oxidation of Fe, oxygen plasma was used. The plasma power was 300 W at an oxygen pressure of 1×10^{-6} mbar. Using these oxygen conditions, BFO was deposited using Fe and oxygen plasma with an overpressure of Bi flux—the growth rate being controlled by the incoming Fe flux. This is the first time that BFO is grown directly on Si with a virtual substrate of STO all in the same system. Growth was monitored throughout using RHEED as shown on Fig. 1(a) that was taken during BFO deposition. It shows a 2-D growth front with a 6-fold surface reconstruction after the growth and anneal of 10 unit cells of BFO film on STO/Si(100) under optimized oxygen pressure of around 1×10^{-6} mbar. For higher and lower O₂ pressures, the RHEED features disappear and then re-appear during annealing. Under non-optimal conditions, XRD shows the formation of second phases such as Bi₂O₃, Fe₂O₃, and FeO. Based on the RHEED pattern, XRD, and XPS data, we optimized the growth conditions. The substrate temperature was $T_s = 650\text{--}700$ °C and we used plasma oxidation with an operating pressure $P_{O_2} \approx 10^{-6}$ Torr where the base pressure of the system before deposition was 10^{-10} Torr. Because of

the use of oxygen plasma, a layer of amorphous SiO₂ is formed at the STO/Si interface up to a thickness of 2.5 nm.

A cross-sectional TEM image of BFO, STO, and the interface between BFO and STO is shown in Figure 1(b). From the selected area diffraction pattern (SADP), shown in Figure 1(c), we get $\alpha = 89.45^\circ \pm 0.20^\circ$ with a and c to a ratio, $c/a = 1.011\text{--}1.015$. BFO grows in a distorted rhombohedral crystal structure. The high angle angular dark field (HAADF) image (Figure 1(c)) which is acquired from an aberration-corrected STEM (JEOL 2100F with probe corrected) confirms the high crystallinity of the films and a clean interface of BFO/STO.

Figure 2(a) shows the XRD θ - 2θ spectrum of a 80 nm thick BFO film and similar spectra were observed for the 20 nm thick films. XRD does not show formation of second phases such as Bi₂O₃, Fe₂O₃, and FeO that we see with non-optimized conditions. All peaks are identified as BFO, STO, or Si. The peaks marked with an asterisk (*) are due to the Al holder and are also observed in the XRD spectrum of the bare Si substrate as shown in the inset of Figure 2(a). The positions of the BFO (200) and (400) peaks show that BFO is grown in the rhombohedral phase and they are consistent with the TEM and SADP results.

XPS is used to determine the formation of the BFO layer on STO and the Fe and Bi oxidation states at various oxygen partial pressures during the initial stages of growth and correlate the results with the RHEED observations. Fig. 2(b) shows XPS survey spectra under the optimized growth conditions. There are XPS photoelectron peaks and the corresponding Auger lines of Fe, O, and Bi as marked. The narrow scan spectra of Bi 4f, Fe 2p, and O 1s are shown in the top portion of Fig. 2(b) and the center of the peaks for Fe 2p_{1/2} (723.8 eV) and Fe 2p_{3/2} (710.9 eV), O 1s (529.7 eV), Bi 4f_{5/2} (164.2 eV) and Bi 4f_{7/2} (158.5 eV) is identified. We

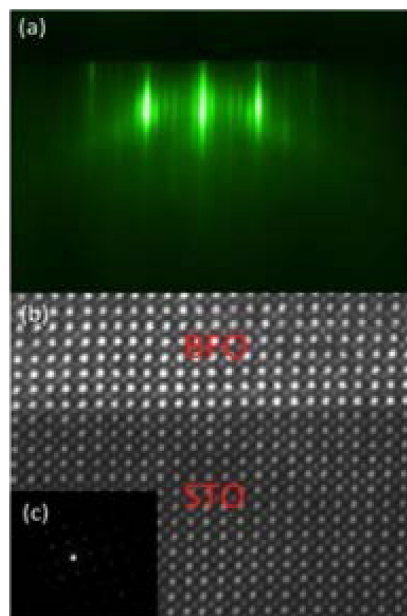


FIG. 1. (a) RHEED image taken during deposition shows a 2-D growth front with a 6-fold surface reconstruction after the growth and anneal of 10 unit cells of BFO film on STO(20 nm)/Si(100), (b) high resolution STEM image showing the sharp interface of BFO/STO, (c) SADP shows BFO grows in a distorted rhombohedral crystal structure.

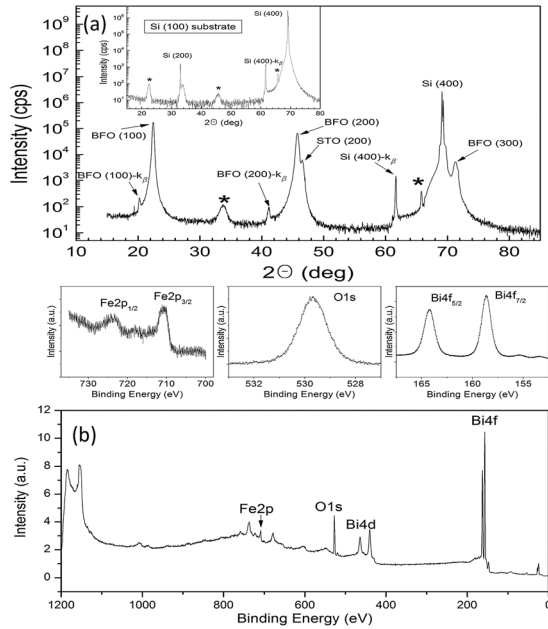


FIG. 2. (a) X-ray diffraction data of BFO(80nm)/STO(20nm)/Si, the BFO (100), (200), and (300) peaks shown correspond to BFO in the rhombohedral phase, all peaks are identified as Si, STO, and BFO and the peaks marked with an asterisk (*) correspond to Al from the sample holder and are present for both the Si substrate and BFO/STO/Si, inset: x-ray diffraction data of the Si(100) substrate. (b) Top: Narrow scan XPS spectra of Bi 4f, Fe 2p, and O 1s, bottom: XPS photoelectron peaks and the corresponding Auger lines of Fe, O, and Bi as marked.

investigated the valence state of Fe using XPS. The 3/2 and 1/2 spin-orbit doublet of Fe 2p were located at 710.9 eV and 723.8 eV, respectively. Both peaks are symmetric and they are associated with the Fe³⁺ valence state.⁸ The smaller peak in between the Fe 2p_{1/2} and Fe 2p_{3/2} peaks is a satellite peak for the Fe³⁺ state. The spin-orbit splitting energy (Δ) of the pure Fe 2p doublet is 12.9 eV, which is comparable to theoretical $\Delta_{\text{Fe } 2p} = 13.6$ eV for Fe₂O₃.⁹ The Fe²⁺ state would give a peak around 709 eV that was not observed.⁸ A mix of the Fe²⁺ and Fe³⁺ state is usually associated with oxygen vacancy defects and degraded electric properties including increased leakage currents and appearance of second phases and it plays an important role in the magnetic and electric properties of the films.¹⁰ XPS shows that Fe in the BFO films grown under optimized conditions is only in the Fe³⁺ state.

The pure Bi 4f doublet consists of two peaks at 158.5 eV for Bi 4f_{7/2} and 164.2 eV for Bi 4f_{5/2}, which are identified as a signal from Bi-O bonds.⁹ The spin-orbit splitting energy (Δ) of the pure Bi 4f doublet is 5.7 eV, which is comparable to theoretical $\Delta_{\text{Bi } 4f} = 5.31$ eV.⁹ The O 1s peak is centered at 529.7 eV that can be ascribed to Fe₂(O 1s)₃ (529.6 eV), Fe-(O 1s) (529.8 eV), and Bi₂-(O 1s)₃ bonds.⁹

The magnetic behavior of the sample is characterized using a VSM. Figures 3(a) and 3(b) show room temperature magnetic hysteresis curves for a 40 nm thick film for H up to 4 kOe (a) and 30 kOe (b). The diamagnetic background due to the Si substrate has been subtracted from all the data. The saturation magnetization per unit volume for a 40 nm thick film was 180 emu/cm³ at an in-plane magnetic field of 8 kOe. This is comparable to the 150 emu/cm³ for BFO (70 nm) thin film

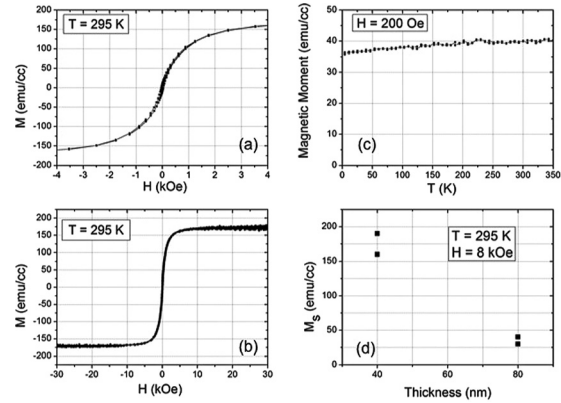


FIG. 3. Room temperature magnetic hysteresis curves for a 40 nm thick film for in plane H up to (a) 4 kOe and (b) 30 kOe, (c) M vs T for H = 200 Oe, in plane showing AF behavior, (d) M_s as a function of the film thickness.

on STO substrate grown by PLD¹ and much higher than the 28 emu/cm³ of BFO (38 nm) grown epitaxially on LAO.¹¹ Figure 3(c) shows the temperature dependence of the magnetization when an in-plane magnetic field, H = 200 Oe, is applied. The BFO films are antiferromagnetic with a residual ferromagnetic behavior and with a Neel temperature that greatly exceeds 350 K, as expected ($T_N = 673$ K). We did not observe any difference in the magnetization when the films were cooled in H = 0 Oe or H = 200 Oe. The saturation magnetization (M_s) decreases with the film thickness and is consistent with the G-type AF due to the spin spiral modulation of 62 nm that is reported in bulk BFO.^{1,12,13} The suppression of M_s for the 80 nm thick film can be explained because of the partial cancellation of magnetic moments when the film is thicker than the 62 nm long cycloidal spin structure.

The surface topography of the samples studied by AFM reveal flat surfaces, a 40 nm film had 0.74 nm rms roughness. The ferroelectric domain structure of the BFO films was observed using out of plane PFM by applying an external driving voltage of 6 Vpp at 6.9 kHz to the tip.

Our results demonstrate the feasibility and the possibility for room temperature magnetoelectric coupling-based devices integrated onto Si CMOS circuitry. Future experiments will detail the effect of the strained STO on the ferroelectric properties of BFO.

Portions of this work were supported by the US ARL and the US ARO under Contract/Grant Number W911NF-10-2-0103 and by AFOSR under Grant No. FA9550-10-1-0133.

- ¹J. Wang, J. B. Neaton, H. Zheng *et al.*, *Science* **299**(5613), 1719 (2003).
- ²W. Eerenstein, N. D. Mathur, and J. F. Scott, *Nature* **442**(7104), 759 (2006).
- ³H. Li, X. Hu, Y. Wei *et al.*, *J. Appl. Phys.* **93**(8), 4521 (2003).
- ⁴R. Droopad, Z. Y. Yu, H. Li *et al.*, *J. Cryst. Growth* **251**(1-4), 638 (2003).
- ⁵T. Zhao *et al.*, *Appl. Phys. Lett.* **84**(5), 750 (2004).
- ⁶M. P. Warusawithana *et al.*, *Science* **324**(5925), 367 (2009).
- ⁷J. Wang, H. Zheng, Z. Ma *et al.*, *Appl. Phys. Lett.* **85**(13), 2574 (2004).
- ⁸P. Mills and J. L. Sullivan, *J. Phys. D: Appl. Phys.* **16**(5), 723 (1983).
- ⁹J. F. Moulder *et al.*, *Handbook of X-ray Photoelectron Spectroscopy* (Physical Electronics, 1992).
- ¹⁰P. Kharel *et al.*, *J. Phys.: Condens. Matter* **21**(3), 036001 (2009).
- ¹¹C.-J. Cheng *et al.*, *Appl. Phys. Lett.* **98**(24), 242502 (2011).
- ¹²M. B. Holcomb *et al.*, *Phys. Rev. B* **81**(13), 134406 (2010).
- ¹³G. J. MacDougall *et al.*, *Phys. Rev. B* **85**(10), 100406 (2012).